Scientia Pharmaceutica

ÖSTERREICHISCHE PHARMAZEUTISCHE GESELLSCHAFT

MDPI

Article

From Molecular Design to In Vivo Validation: Integrated Efficacy and Safety Profiling of Orotic Acid–1,2,4-Triazole Hybrids with Wound-Healing Activity

Yuriy Karpenko [1,*], Volodymyr Parchenko [1], Borys Kyrychko [2], Liudmyla Kucherenko [3], Olena Ishchenko [4], Iryna Pukhalska [5], Tetiana Chetvertak [6], Daria Safronova [5] and Mykola Shumeiko [7]

[1] Department of Toxicological and Inorganic Chemistry, Zaporizhzhia State Medical and Pharmaceutical University, 69035 Zaporizhzhia, Ukraine; parchenko@ukr.net
[2] Department of Surgery and Obstetrics, Poltava State Agrarian University, 36003 Poltava, Ukraine; borys.kyrychko@pdau.edu.ua
[3] Department of Pharmaceutical, Organic and Bioorganic Chemistry, Zaporizhzhia State Medical and Pharmaceutical University, 69035 Zaporizhzhia, Ukraine; kucherenko.l.i@mphu.edu.ua
[4] Department of Industrial Pharmacy, Kyiv National University of Technologies and Design, 01011 Kyiv, Ukraine; ishhenko.ov@knutd.edu.ua
[5] Department of Drug Technology, Zaporizhzhia State Medical and Pharmaceutical University, 69035 Zaporizhzhia, Ukraine; pukhalska.i.o@zsmu.edu.ua (I.P.); romaningena0@gmail.com (D.S.)
[6] Department of Chemistry and Chemical Education, Bogdan Khmelnitsky Melitopol State Pedagogical University, 69035 Zaporizhzhia, Ukraine; tetiana.chetvertak@mspu.edu.ua
[7] Department of Pharmacy and Industrial Technology of Drugs, Bogomolets National Medical University, 01601 Kyiv, Ukraine; shumeiko@nmu.ua
* Correspondence: karpenko.y.v@gmail.com; Tel.: +380-639734427

Abstract

Chronic and difficult-to-heal wounds require topical agents that combine reparative activity with favorable local disposition and an acceptable preliminary safety profile. This study evaluated three orotic acid–1,2,4-triazole hybrids (1–3) using an integrated computational and experimental workflow. Accelerated weight histogram simulations were performed in an atomistic human stratum corneum lipid model; acute toxicity was assessed by in silico rat LD_{50} prediction, 96 h *Danio rerio* LC_{50} testing, and OECD 425 oral testing in rats. Compounds selected on the basis of toxicity were incorporated into electrospun polyvinylpyrrolidone K-30 dressings and evaluated in a rat excisional wound model. Compound **1** showed pronounced lipid partitioning and potential intralamellar retention, whereas compounds **2** and **3** encountered broad membrane-interior free-energy barriers. Compound **2** had the least favorable acute-toxicity profile and was excluded. By day 8, wound area decreased by 89.0% with compound **1** and 78.6% with compound **3**, versus 70.5% with the drug-free vehicle dressing ($p < 0.001$ for both comparisons). Neither treatment caused clinically evident deterioration or a consistent biochemical pattern of marked hepatic or renal dysfunction, although hematological and compound-specific biochemical changes were observed. The compound **1**-loaded dressing therefore warrants further mechanistic, histological, and longer-term safety evaluation as the lead formulation.

Keywords: wound healing; orotic acid; 1,2,4-triazole; electrospun dressings; polyvinylpyrrolidone; acute toxicity; stratum corneum

Check for updates

Academic Editor: Thierry Besson

Received: 3 September 2026
Revised: 8 October 2026
Accepted: 12 October 2026
Published: 14 October 2026

Copyright: © 2026 by the authors. Published by MDPI on behalf of the Österreichische Pharmazeutische Gesellschaft. Licensee MDPI, Basel, Switzerland. This article is an open access article distributed under the terms and conditions of the Creative Commons Attribution (CC BY) license.

1. Introduction

Loss of skin integrity initiates a complex reparative response aimed at restoring barrier function and protecting the underlying tissues. Although many acute wounds

heal without major intervention, extensive injuries and wounds complicated by infection, ischemia, metabolic disease, aging, or persistent inflammation may fail to heal and impose a substantial clinical and socioeconomic burden. In Ukraine, the need for improved wound care has become particularly urgent since Russia's full-scale invasion in February 2022, as high-energy combat trauma has resulted in complex extremity and soft-tissue wounds that present considerable challenges for surgical treatment and subsequent tissue repair [1]. This problem is further aggravated by infectious complications and antimicrobial resistance: in a recent cohort of 73 wounded Ukrainian service members, bacteria were isolated from 56.2% of wound samples, and 84.6% of the recovered isolates were multidrug resistant [2]. These circumstances make the development of effective wound-healing agents and advanced dressing materials not only a global biomedical objective but also an immediate healthcare priority for Ukraine, underscoring the need for accessible topical therapies that can promote wound closure while maintaining an acceptable safety profile.

Cutaneous wound healing is generally described as a sequence of overlapping phases—hemostasis, inflammation, proliferation, and remodeling. In practice, these phases form a continuous and highly coordinated biological network involving platelets, neutrophils, monocytes and macrophages, keratinocytes, fibroblasts, endothelial cells, extracellular matrix components, cytokines, growth factors, and proteolytic enzymes [3]. Successful healing therefore depends not on the complete suppression of inflammation but on its appropriate resolution and transition to the proliferative phase. Failure of this transition, together with persistent immune-cell activation, oxidative imbalance, impaired angiogenesis, and dysregulated extracellular matrix turnover, is characteristic of hard-to-heal wounds [4,5].

Small molecules are attractive in this context because their structures, physicochemical properties, and target interactions can be systematically optimized. Compared with proteins and growth factors, they may also be less susceptible to degradation in the highly proteolytic wound environment and can be incorporated into relatively simple topical delivery systems. The feasibility of this strategy has been demonstrated with the triazolothiadiazine derivative UCUF-965, a small-molecule positive allosteric modulator of CXCR4 that enhanced angiogenesis and reduced wound-closure time in diabetic mice [6].

The 1,2,4-triazole scaffold [7] is particularly amenable to such structural modification and can support hydrogen-bonding and heteroaromatic interactions as well as the introduction of sulfur-containing substituents with tunable physicochemical properties [8]. Orotic acid is an endogenous intermediate in de novo pyrimidine biosynthesis [9]. Combining a pyrimidine-2,4-dione core with an S-substituted 1,2,4-triazole moiety therefore provides a chemically rational hybrid scaffold containing multiple hydrogen-bond donors and acceptors, a tunable sulfur-containing region, and positions suitable for modulating lipophilicity and steric complementarity. Systemic nutritional and metabolic status may also influence tissue recovery, and the roles of vitamins, magnesium, and trace elements have been discussed in the context of post-disease rehabilitation [10].

Our previous studies provided a preliminary biological rationale for the further development of this chemical platform. Compound **1** in the present study corresponds to compound **17** previously shown to exhibit pronounced MMP-2/MMP-9 modulation with preferential activity toward MMP-9 [11]. In a related series of 1,2,4-triazole–thiopyrimidine derivatives, several S-substituted compounds exhibited experimentally confirmed antiradical activity [12]. In addition, compound **2** in the present study corresponds to compound **17** evaluated in our previous cyclooxygenase-inhibition study [13]. Collectively, these findings indicate that this chemical platform can support pharmacological effects relevant to extracellular-matrix remodeling, oxidative balance, and inflammatory regulation. These prior findings provided the pharmacological background for advancing the selected com-

pounds to comparative toxicity assessment, cutaneous-disposition modeling, and in vivo evaluation of wound-area reduction.

The pharmaceutical carrier is another important determinant of topical activity. Electrospinning can produce highly porous fibrous materials with a large surface-to-volume ratio and the capacity to incorporate small-molecule therapeutic agents [14,15]. Such materials can provide close contact with irregular wound surfaces and enable localized delivery while limiting unnecessary systemic exposure. Depending on the polymer composition and fiber architecture, electrospun systems may also influence hydration, drug dissolution, release kinetics, and interactions with wound exudate [16]. Polyvinylpyrrolidone (PVP) is a nonionic, hydrophilic pharmaceutical polymer that can be readily processed from aqueous or hydroalcoholic solutions. Electrospun PVP-containing systems have been used to molecularly disperse poorly soluble drugs and enhance their dissolution or release [17,18]. Its rapid hydration makes PVP K-30 suitable as a platform for localized delivery.

Recent advances in wound-dressing research illustrate the increasing multifunctionality of topical biomaterial systems. For example, intrinsically antibacterial cationic hydrogels have been shown to combine bacterial killing with hemostatic activity, modulation of macrophage polarization, collagen deposition, and neovascularization in experimental wound models [19]. More broadly, nanomaterial-based wound dressings are evolving from passive wound coverings toward multifunctional therapeutic and diagnostic platforms capable of supporting wound management and, in some cases, monitoring the healing environment [20]. In contrast to these multifunctional biomaterial-centered approaches, the present study focuses on the pharmacological selection of structurally defined small-molecule orotic acid–1,2,4-triazole hybrids and their incorporation into a comparatively simple PVP K-30 fibrous carrier. The distinguishing feature of our workflow is the integration of molecular-level cutaneous disposition modeling, complementary acute-toxicity assessment, formulation into an electrospun carrier, and subsequent in vivo evaluation of macroscopic wound-area reduction.

Cutaneous disposition must also be considered when prioritizing molecules for topical development. The stratum corneum is the principal permeability barrier of intact skin and consists of corneocytes surrounded by a highly organized intercellular lipid matrix dominated by ceramides, cholesterol, and free fatty acids [21]. Molecular dynamics simulations using such models can characterize the free-energy cost of transferring a molecule from water into and across different regions of the lipid lamella and have demonstrated meaningful correlations with experimentally measured skin permeability [22]. Enhanced-sampling methods, such as the accelerated weight histogram (AWH) method, can improve the exploration of these high-barrier processes by combining spatial and alchemical reaction coordinates [23]. The resulting potential-of-mean-force profiles provide information on membrane permeation barriers, favorable intralamellar locations, and possible lipid-phase retention.

2. Materials and Methods

2.1. Chemistry

Compounds **1**–**3** were selected for the present study based on the encouraging findings obtained in our previous investigations, which demonstrated their potential for further development as wound-healing agents [11,13]. They were previously synthesized and characterized at the Department of Toxicological and Inorganic Chemistry using our reported approach to the preparation of 6-(5-mercapto-4R-4H-1,2,4-triazol-3-yl)pyrimidine-2,4(1*H*,3*H*)-dione derivatives [24]. Accordingly, the detailed synthetic procedures and analytical characterization data are not repeated here. The chemical structures of the investigated compounds are shown in Figure 1.

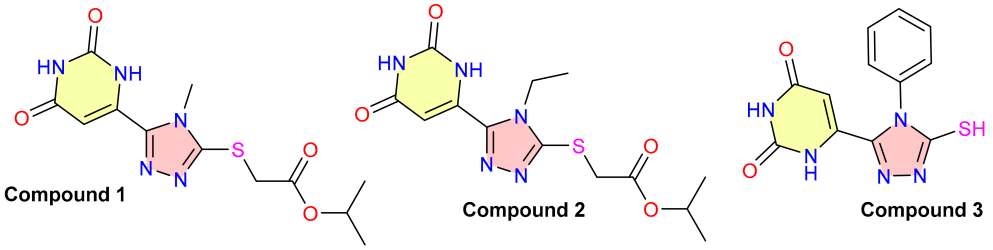


Figure 1. Chemical structures of the orotic acid–1,2,4-triazole hybrids investigated in this study.

2.2. Molecular Dynamics Model of the Stratum Corneum Lipid Barrier

Free energy profiles of compounds throughout the stratum corneum lipid matrix were calculated using the accelerated weight histogram (AWH) method implemented in GROMACS 2025.3. An atomistic model of the human stratum corneum lipid lamella containing ceramides, cholesterol, free fatty acids, and explicit water was constructed with reference to previously reported atomistic models and simulation studies of stratum corneum lipid organization and permeation [25–27]. Lipids and permeants were described using CHARMM36-compatible parameters and CGenFF parameters, respectively [28,29]. Compound **3** was modeled as the neutral thiol tautomer (R–SH). Although sulfur-containing heterocycles may undergo thione–thiol tautomerism depending on their molecular environment, as previously demonstrated for related heterocyclic thiones [30], only the thiol form was explicitly considered in the present simulations.

A two-dimensional AWH protocol was used, combining ligand displacement along the membrane normal (z = −5.215 to +5.215 nm) with an alchemical bond coordinate comprising 21 states [31]. For each compound, two communicating AWH walkers were simulated for 120 ns each, corresponding to an aggregate sampling time of 240 ns per compound. The walkers shared a common adaptive bias and were therefore not treated as statistically independent replicas. PMF profiles were extracted at 10 ns intervals and normalized to the pooled mean free energy of the terminal aqueous regions. Convergence was assessed by comparison of the 10–110 ns profiles with the final 120 ns profile and by evaluation of agreement between the two terminal aqueous regions. The RMS deviations between the 110 and 120 ns profiles were 1.89, 1.75, and 1.94 kJ mol^{-1} for compounds **1**, **2**, and **3**, respectively. Accordingly, the PMF profiles were interpreted as semi-quantitative comparative estimates rather than as fully converged absolute free-energy profiles.

The calculated PMFs were used to compare membrane affinity and free energy barriers associated with compound transport across the lipid lamella. Absolute permeability coefficients were not calculated as this additionally requires an independently validated position-dependent diffusion coefficient D_z [32]. Detailed information on the molecular composition, permeant parameters, two-dimensional AWH setup, PMF normalization, and stability-assessment procedures is provided in Section S1 and Tables S1 and S2 of the Supplementary Materials.

2.3. In Silico and Experimental Assessment of Acute Toxicity

The acute toxicity of compounds **1–3** was evaluated using complementary computational and experimental approaches. The assessment included in silico prediction of rat oral toxicity, a 96 h acute toxicity test in adult *Danio rerio*, and acute oral toxicity testing of all three compounds in rats.

The chemical structures of compounds **1–3**, represented as canonical SMILES strings, were analyzed using the U.S. EPA Toxicity Estimation Software Tool (TEST, version 5.1.2) and the pkCSM web platform [33–35]. Rat oral LD_{50} values in TEST were obtained using the consensus QSAR method [36,37]. The pkCSM model provides rat oral LD_{50} estimates

in mol/kg; therefore, these values were converted to mg/kg using the molecular weight of each compound.

Acute aquatic toxicity was evaluated in clinically healthy adult *Danio rerio* using a protocol adapted from OECD Test Guideline 203 [38]. Before testing, the fish were acclimatized to the laboratory conditions. Fish were maintained in aerated tap water purified through an activated-carbon filter at 26.5 °C and pH 7.3 ± 0.3. Temperature, pH, and dissolved oxygen concentration were monitored throughout the experiment.

Fish were randomly allocated to six nominal test concentrations (5, 10, 18, 34, 65, and 100 mg/L), a negative-control group, and a vehicle-control group, with seven fish per concentration or control group. Each group was maintained in 3 L of exposure medium. To facilitate dispersion, the test compounds were initially mixed with 0.067 mL of Tween 80 before dilution with water to the required nominal concentration. This corresponded to a final Tween 80 concentration of approximately 0.0022% (*v*/*v*). The same volume of Tween 80 was added to the vehicle-control medium, whereas the negative-control medium contained neither the test compound nor Tween 80. The exposure concentrations of the test compounds were nominal and were not analytically verified. No mortality was observed in either the negative-control or vehicle-control group during the 96 h exposure period (0/7 fish in each group). Exposure was conducted under static conditions for 96 h without feeding. Mortality was recorded after 24, 48, 72, and 96 h. Fish were considered dead when spontaneous movement, opercular movement, and response to gentle mechanical stimulation of the caudal peduncle were absent; dead fish were removed immediately. Changes in swimming activity and equilibrium, respiratory movements, responsiveness to external stimuli, and the occurrence of exophthalmia, hemorrhage, excessive mucus secretion, or edema were additionally recorded. Cumulative mortality at each concentration was expressed as the number and percentage of dead fish at 24, 48, 72, and 96 h. The complete concentration–mortality data are provided in Section S2 of the Supplementary Materials. The 96 h LC_{50} values were calculated from the concentration-mortality relationships using the Quest Graph™ LC_{50} Calculator provided by AAT Bioquest, Inc. (Pleasanton, CA, USA). [39].

The acute oral toxicity of compounds **1**–**3** was evaluated in clinically healthy adult Wistar male rats weighing 200–240 g according to the main-test up-and-down procedure described in OECD TG 425 [40]. Each compound was investigated in a separate sequential experiment. Before administration, the animals were fasted overnight while retaining unrestricted access to water. The test compounds were administered once by oral gavage. Animals were dosed individually and sequentially, generally at intervals of at least 48 h. The starting dose for each compound was selected one step below the best preliminary estimate of its LD_{50}. Subsequent dose levels were generated automatically by the AOT425StatPgm software developed by Westat for the U.S. EPA [41]. If an animal survived, the next animal received the subsequent higher dose; if the animal died or reached a predefined humane endpoint, the next animal received the subsequent lower dose. Dosing was continued until the software-defined stopping criterion was met. The complete dose sequences, individual short- and long-term outcomes, stopping criteria, LD_{50} estimates, and 95% confidence intervals for all three compounds are provided in Section S2 of the Supplementary Materials. Animals were observed closely during the first 4 h after administration, periodically during the first 24 h, and at least once daily for 14 days. Rat oral LD_{50} values and their 95% confidence intervals were calculated by AOT425StatPgm using the maximum-likelihood procedure implemented for OECD TG 425 [40]. Acute oral toxicity categories were assigned from the experimental LD_{50} point estimates according to the criteria of the Globally Harmonized System of Classification and Labelling of Chemicals [42].

All procedures involving animals were conducted in accordance with national bioethical requirements, the European Convention for the Protection of Vertebrate Animals Used for Experimental and Other Scientific Purposes (ETS No. 123), Directive 2010/63/EU, and the principles of replacement, reduction, and refinement [43,44]. The study protocol was reviewed and approved by the Commission on Bioethics of Poltava State Agrarian University (Protocol No. 1 C/I, approved on 12 January 2026).

2.4. Preparation of Fibrous Materials by Electrospinning

Nonwoven fibrous materials were fabricated by capillary electrospinning using a laboratory-scale setup. The spinning solution was prepared by dissolving polyvinylpyrrolidone K-30 (PVP K-30) in 96% ethanol to obtain a final polymer concentration of 40% (*w*/*w*) [45].

Compounds **1** and **3** were separately incorporated into the corresponding PVP K-30 solutions at a loading of 1% (*w*/*w*) relative to the mass of the polymer. An identically prepared drug-free PVP K-30 solution was used to produce the vehicle-control dressing. Each mixture was thoroughly stirred until a visually homogeneous spinning solution was obtained. During preliminary optimization, the applied voltage was varied from 5 to 60 kV. The samples used in subsequent studies were produced at an applied voltage of 55–60 kV and a tip-to-collector distance of 17–20 cm. Under these conditions, stable jet formation and deposition of visually uniform fibrous materials without pronounced macroscopic defects were observed; SEM examination further confirmed the formation of an interconnected fibrous network (Figure 2C). The surface morphology of the electrospun material was additionally examined by scanning electron microscopy using a MIRA3 TESCAN instrument (TESCAN, Brno, Czech Republic).

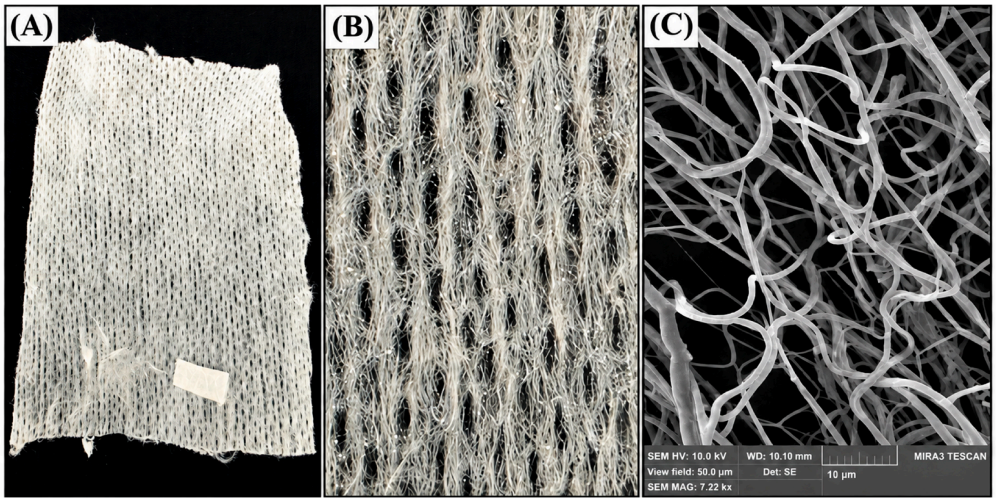


Figure 2. Appearance and morphology of the PVP K-30-based fibrous material prepared by electrospinning: (**A**) overall view of the sample; (**B**) enlarged view of its surface; and (**C**) representative SEM micrograph of the fibrous structure. Scale bar: 10 µm.

2.5. Excisional Wound Model and Topical Treatment

Fifteen clinically healthy adult Wistar male rats weighing 200–240 g were housed under standard conditions at the Educational, Research, and Production Clinic of Veterinary Medicine of Poltava State Agrarian University (Poltava, Ukraine), with free access to standard laboratory chow and water. After an acclimatization period of 14 days, the animals were allocated to three groups of five rats each.

The procedure was performed under general anesthesia using a Veta 5 veterinary anesthesia system operated in ACGO mode. Anesthesia was maintained with isoflurane

following premedication with tiletamine-zolazepam (Zoletil®) and medetomidine. After hair removal and antiseptic preparation of the intervention area, a standardized full-thickness excisional skin wound was created on the lateral abdominal wall [46], resulting in a mean baseline wound area of 1.73 ± 0.01 cm^2.

Immediately after wound induction, the animals received one of the following PVP K-30-based electrospun fibrous dressings: a dressing containing compound **1**, a dressing containing compound **3**, or an identically prepared drug-free dressing used as the vehicle control. The dressings prepared as described in Section 2.4 were cut into 20 × 40 mm pieces weighing approximately 200 ± 12 mg. Compound loading was defined as 1% (*w*/*w*) relative to the dry mass of PVP K-30. Accordingly, a dressing containing approximately 198 mg of PVP K-30 contained a theoretical compound amount of approximately 1.98 mg. This value represents theoretical loading based on formulation composition and was not determined analytically. The dressing was placed directly in contact with the wound bed and secured to the surrounding shaved intact skin using medical adhesive tape without applying excessive pressure. Dressings were replaced once daily throughout the active treatment period up to Day 8. Thereafter, the animals were monitored until Day 14 to document the final macroscopic outcome of wound closure. Additional details of the dressing application and fixation procedure are provided in Section S3 of the Supplementary Materials and illustrated in Figure S1.

Wound area was quantitatively assessed immediately after wound induction and on Days 4 and 8. An additional macroscopic assessment was performed on Day 14 to document the final appearance and closure status of the wounds. Before each assessment, the adhesive tape and dressing were gently removed, and the wound was photographed for macroscopic documentation. The maximum wound length (L) and width (W) were measured in centimeters, and the wound area was estimated using Kundin's formula [47]:

$$S = L \times W \times 0.785$$

where S is the wound area in cm^2. Wound-area reduction was calculated relative to baseline as follows:

$$\text{Wound} - \text{area reduction}(\%) = \frac{S_0 - S_t}{S_0} \times 100$$

where (S_0) is the baseline wound area and (S_t) is the area at the corresponding assessment time. After the day-4 assessment, a fresh dressing of the corresponding type was applied and secured in the same manner. General clinical condition, activity, food and water consumption, dressing position, and macroscopic wound appearance were monitored daily.

All animal procedures complied with national bioethical requirements, the European Convention ETS No. 123, Directive 2010/63/EU, and the principles of the 3Rs [43,44]. The study protocol was reviewed and approved by the Commission on Bioethics of Poltava State Agrarian University (Protocol No. 1 C/I, approved on 12 January 2026).

2.6. Blood Sampling and Hematological and Biochemical Analyses

On Day 8, immediately after the final quantitative wound-area assessment, blood samples were collected from the tail vein of each animal (n = 5 per group). Animals were subsequently monitored macroscopically until Day 14. Hematological parameters included white blood cell (WBC) count, red blood cell (RBC) count, hemoglobin (HGB) concentration, hematocrit (HCT), mean corpuscular volume (MCV), mean corpuscular hemoglobin (MCH), mean corpuscular hemoglobin concentration (MCHC), red blood cell distribution width (RDW), platelet (PLT) count, mean platelet volume (MPV), erythrocyte sedimentation rate (ESR), and leukocyte differential count. Serum biochemical

parameters included albumin, total protein, alkaline phosphatase (ALP), alanine aminotransferase (ALT), aspartate aminotransferase (AST), lactate dehydrogenase (LDH), gamma-glutamyl transferase (GGT), creatinine, urea, glucose, total cholesterol, triglycerides, α-amylase, total and direct bilirubin, uric acid, inorganic phosphorus and total calcium. Indirect bilirubin and the albumin-to-globulin ratio were calculated from the corresponding measured parameters.

Hematological analyses were performed at the specialized veterinary laboratory "Bald" (Kyiv, Ukraine), whereas serum biochemical analyses were conducted at the biochemical laboratory of Poltava City Hospital No. 4 (Poltava, Ukraine).

2.7. Statistical Analysis of the Results

Wound-area data were analyzed using a two-way mixed repeated-measures ANOVA, with treatment group as the between-subject factor and time as the within-subject factor, including the group × time interaction. Normality of model residuals was assessed using the Shapiro–Wilk test, homogeneity of variances at each time point using Levene's test, and sphericity using Mauchly's test; no significant violations of these assumptions were detected. Between-group comparisons at individual time points were additionally performed using one-way ANOVA followed by Dunnett's multiple-comparisons test, with the vehicle-control group as the reference. Effect sizes were expressed as partial η^2 for the repeated-measures ANOVA and η^2 for the one-way ANOVA, and mean differences are reported with 95% confidence intervals. Hematological, leukocyte differential, and serum biochemical parameters measured at the terminal time point were compared between each treatment group and the vehicle-control group using the unpaired Student's *t*-test. No formal a priori power calculation was performed because the in vivo study was exploratory; accordingly, effect sizes and 95% confidence intervals were emphasized to support interpretation of the magnitude and precision of the observed effects. Data are presented as mean ± SEM, with five biologically independent animals per group, and a two-sided p value < 0.05 was considered statistically significant. Statistical analyses were performed using BioStat LE version 7 (AnalystSoft Inc., Walnut, CA, USA) and MedCalc version 23.7.1 (MedCalc Software Ltd., Ostend, Belgium) [48,49]. Individual animal-level wound-area measurements and detailed statistical results are provided in Section S4 of the Supplementary Materials.

3. Results and Discussion

3.1. Free-Energy Profiles and Predicted Cutaneous Disposition

Before experimental safety and efficacy testing, accelerated weight histogram (AWH) simulations were used to compare the thermodynamic behavior of the investigated compounds within an atomistic human stratum corneum lipid model. Potential of mean force (PMF) profiles were obtained for compounds **1–3** (Figure 3). Each system was sampled using two communicating AWH walkers for 120 ns per walker.

The PMF profiles describe the free-energy changes associated with transfer from the aqueous phase into different regions of the lipid lamella. They therefore provide comparative information on lipid affinity, thermodynamic barriers to membrane entry, and possible intralamellar retention. Because position-dependent diffusion coefficients were not calculated, the results should not be interpreted as absolute permeability coefficients.

The three compounds displayed markedly different free-energy profiles (Table 1). Compound 1 exhibited the most favorable interaction with the lipid matrix, with a global PMF minimum of -24.78 kJ mol^{-1} at (z = +1.17) nm and a comparatively low free-energy value of +3.56 kJ mol^{-1} near the membrane center.

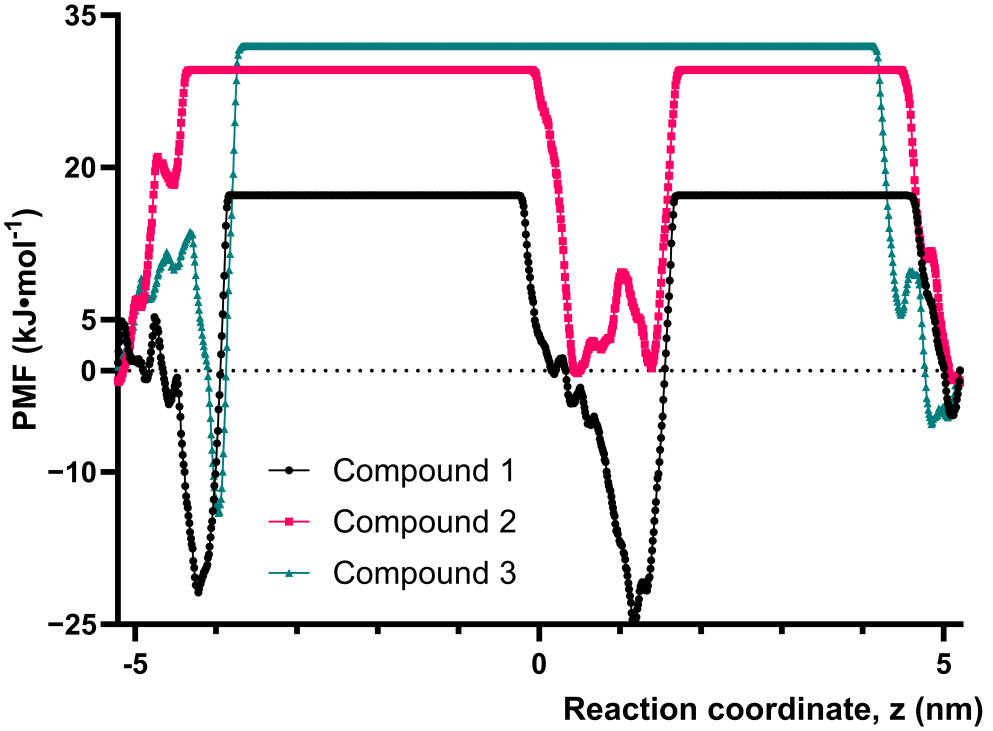


Figure 3. Potential of mean force profiles of compounds **1**–**3** across the human stratum corneum lipid model. The reaction coordinate z represents the displacement of the compound relative to the lipid lamella along the membrane normal. PMF values were extracted from the fully interacting state of the two-dimensional accelerated weight histogram simulations and normalized to the mean free energy of the terminal aqueous regions. Each profile was obtained from two communicating AWH walkers simulated for 120 ns per walker. Compound **1** exhibited pronounced stabilization within the lipid phase, whereas compounds **2** and **3** displayed broad free-energy barriers in the membrane interior.

Table 1. Summary of potential of mean force (PMF) extrema and central free-energy values for compounds **1**–**3** across the human stratum corneum lipid model.

Compound	Global PMF Minimum, kJ mol^{-1}	Position of Minimum, nm	Maximum PMF, kJ mol^{-1}	Position of Maximum, nm	PMF Near Membrane Centre, kJ mol^{-1}
1	−24.78	+1.172	+17.27	−3.777	+3.56
2	−1.18	+5.205	+29.62	−4.260	+27.57
3	−14.03	−3.968	+31.96	−3.616	+31.96

Note: PMF values were normalized to the mean free energy of the terminal aqueous regions. Positions correspond to the reaction coordinate (z) along the membrane normal.

These findings indicate that transfer of compound **1** from the aqueous phase into a specific intralamellar region was thermodynamically favorable. This behavior suggests pronounced lipid partitioning and the potential formation of a local intramembrane reservoir. However, a deep free-energy minimum may also promote retention within the lipid phase; therefore, strong lipid affinity should not be equated with rapid passage across the entire membrane.

In contrast, compound **2** did not exhibit a pronounced favorable minimum within the lipid phase. Its PMF increased upon entry into the lipid lamella, reaching a maximum of +29.62 kJ mol^{-1}, while the free energy near the membrane center remained high at +27.57 kJ·mol^{-1}. The broad high-energy region indicates that passive transfer of compound **2** through the ordered stratum corneum lipids is thermodynamically unfavorable.

Compound **3**, modeled in its neutral thiol form, displayed the highest central free-energy barrier, reaching +31.96 kJ·mol^{-1}. An apparent minimum of −14.03 kJ·mol^{-1} was detected near z = −3.97 nm; however, it was located immediately adjacent to a steep and incompletely stabilized PMF transition. This feature should therefore not be regarded as a confirmed membrane-binding site. Although the same neutral thiol form was used in the experimental studies, its protonation state and local disposition under biological conditions may still depend on the local pH and surrounding microenvironment.

Overall, compound **1** showed the strongest predicted lipid partitioning and potential intramembrane retention, whereas compounds **2** and **3** encountered broad free-energy barriers of approximately 30–32 kJ mol^{-1} within the membrane interior. The difference between compounds **2** and **3** was relatively small and should not be overinterpreted. The progressive decrease in the RMS differences between successive PMF profiles indicated an approach toward stabilization; nevertheless, residual differences of 1.75–1.94 kJ mol^{-1} remained between 110 and 120 ns. Accordingly, the calculated profiles were interpreted as semi-quantitative comparative estimates, and emphasis was placed on the consistent qualitative differences among the compounds rather than on the exact magnitudes of individual PMF extrema.

These findings identified distinct patterns of predicted cutaneous disposition but were not used as an exclusion criterion. The stratum corneum model used in the present study represents the permeability barrier of intact skin and therefore does not reproduce the environment of a full-thickness open wound, in which the stratum corneum is absent. Consequently, the PMF profiles should not be interpreted as direct predictors of compound availability within the wound bed or as predictors of therapeutic efficacy. Rather, these simulations provide comparative information on the interaction of the investigated compounds with intact or regenerating cutaneous lipid domains and may be most relevant to periwound skin, wound margins, and newly re-epithelialized regions during the healing process. Furthermore, favorable membrane disposition does not necessarily imply an acceptable safety profile. Consequently, all three compounds were subsequently subjected to complementary computational and experimental acute-toxicity assessment, which served as the principal stage for selecting candidates for the wound-healing study.

3.2. Acute-Toxicity Assessment

The acute toxicity of compounds **1**–**3** was evaluated using complementary in silico and experimental approaches (Table 2). The rat oral LD_{50} values predicted by TEST and pkCSM were generally consistent with the experimentally derived estimates, although the degree of agreement differed among the compounds.

Table 2. In silico-predicted rat oral toxicity, experimental acute oral toxicity in rats, and 96 h acute toxicity in *Danio rerio* for compounds **1**–**3**.

Compound	TEST Rat Oral LD_{50}, mg/kg	pkCSM Rat Oral LD_{50}, mg/kg	Toxicity	
			Danio Rerio LC_{50}, mg/L	Rat Oral LD_{50}, mg/kg
1	1503.06	1573.26	40.4486	1570 (1030–2430 *)
2	719.38	1112.9	6.6462	1110 (408.1–1600 *)
3	1199.65	2788.9	23.1785	1800 (1760–2800 *)

Note: * Values in parentheses represent 95% confidence intervals calculated using AOT425StatPgm.

For compound **1**, the TEST and pkCSM predictions were 1503.06 and 1573.26 mg/kg, respectively, and closely corresponded to the experimental LD_{50} of 1570 mg/kg (95% CI: 1030–2430 mg/kg). This close agreement indicates good consistency between the computational models and the in vivo outcome.

For compound **2**, pkCSM predicted an LD_{50} of 1112.9 mg/kg, which was almost identical to the experimental estimate of 1110 mg/kg (95% CI: 408.1–1600 mg/kg). In contrast, TEST predicted a lower LD_{50} of 719.38 mg/kg, suggesting greater acute toxicity. Nevertheless, both computational models correctly identified compound **2** as the most toxic compound within the investigated series. Compound **3** showed the greatest intermodel variability: TEST predicted an LD_{50} of 1199.65 mg/kg, whereas the pkCSM estimate was 2788.9 mg/kg. The experimentally calculated LD_{50} of 1800 mg/kg was intermediate between these predictions.

Based on the experimental point estimates, the order of acute oral toxicity in rats was compound **2** > compound **1** > compound **3**. All three compounds had LD_{50} values within the range of 300–2000 mg/kg and could therefore be assigned to GHS acute oral toxicity Category 4.

The acute toxicity pattern in *Danio rerio* was consistent with the rat results in identifying compound **2** as the most toxic member of the series. Its LC_{50} was 6.6462 mg/L, compared with 23.1785 mg/L for compound 3 and 40.4486 mg/L for compound 1. Thus, compound 2 was approximately 3.5-fold more toxic than compound **3** and 6.1-fold more toxic than compound **1** in the fish model. Compound **3** exhibited intermediate aquatic toxicity, whereas compound **1** demonstrated the most favorable fish toxicity profile.

Taken together, the computational predictions and experimental findings consistently identified compound **2** as the least favorable candidate in terms of acute toxicity. In contrast, compounds **1** and **3** demonstrated comparatively more favorable toxicity profiles in both rats and *Danio rerio*. Thus, acute-toxicity assessment provided the principal basis for candidate selection: compounds **1** and **3** were advanced to topical evaluation, whereas compound **2** was excluded from further in vivo investigation.

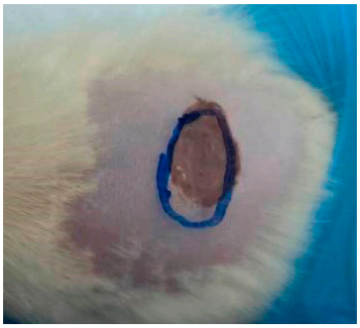
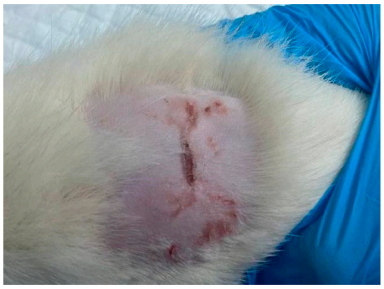
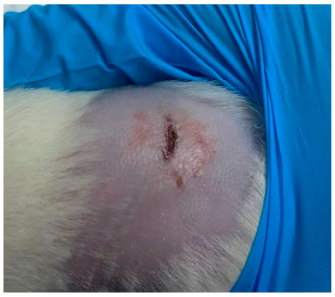
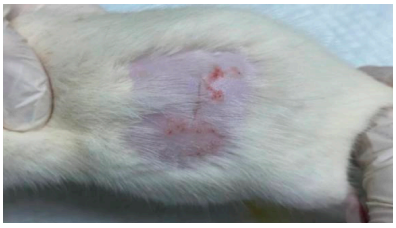
In the present workflow, acute oral toxicity was used as an early comparative hazard-ranking tool for candidate prioritization rather than as a surrogate for topical safety. The relevance of oral LD_{50} values to repeated application on an open wound is inherently limited because local tolerability, dermal or wound-bed exposure, systemic absorption from damaged skin, and repeated topical toxicity were not directly assessed. Accordingly, dedicated studies of local tolerability, systemic exposure, and repeated-dose topical safety will be required before further pharmaceutical development.

3.3. In Vivo Wound-Healing Activity of the Selected Compounds

Based on the acute-toxicity findings, compounds **1** and **3** were incorporated separately into PVP K-30-based electrospun fibrous dressings and evaluated in the rat excisional wound model. An identically prepared compound-free PVP K-30 dressing was used as the vehicle control. This design enabled comparison of the wound-healing effects of the two selected compounds, which combined comparatively favorable acute-toxicity profiles with distinct patterns of predicted interaction with the stratum corneum lipid matrix.

Throughout the experimental period, the animals in all groups remained active and mobile and maintained normal food intake. Topical application of the tested materials containing compound **1** or compound **3** was not associated with any clinically evident deterioration in the general condition of the animals. Changes in wound area are presented in Table 3. Planimetric assessment performed on days 0, 4, and 8 revealed differences in the rate of wound-area reduction among the study groups.

Table 3. Macroscopic wound appearance and planimetric wound area (cm^2) in rats treated with PVP K-30-based fibrous dressings containing compounds **1** and **3** and in the vehicle-control group.

Date	Vehicle Control	Compound 1	Compound 3
Day 0			
	1.73 ± 0.01	1.73 ± 0.01	1.73 ± 0.01
Day 4			
	1.59 ± 0.02	0.75 ± 0.01 ***	1.19 ± 0.01 ***
Day 8			
	0.51 ± 0.01	0.19 ± 0.02 ***	0.37 ± 0.01 ***
Day 14			

Data are presented as mean ± SEM (n = 5 biologically independent animals per group). Between-group comparisons at each time point were performed using one-way ANOVA followed by Dunnett's multiple-comparisons test, with the vehicle-control group as the reference. *** $p < 0.001$ versus the vehicle-control group at the corresponding time point.

The most pronounced reduction in wound area was observed in animals treated with compound **1**. By day 4, the wound area had decreased from 1.73 ± 0.01 to 0.75 ± 0.01 cm^2, representing a 56.6% reduction from baseline. In contrast, the vehicle-control group showed a reduction of only 8.1%, from 1.73 ± 0.01 to 1.59 ± 0.02 cm^2. The difference compared with the vehicle-control group was statistically significant ($p < 0.001$). By day 8, the wound area in the compound **1** group had decreased to 0.19 ± 0.02 cm^2, corresponding to an 89.0% reduction from baseline, and was significantly smaller than that observed in the vehicle-control group (0.51 ± 0.01 cm^2; $p < 0.001$).

The pronounced wound-closure effect of compound **1** was accompanied by a higher relative proportion of monocytes. However, because the total WBC count was lower in this group, the calculated absolute monocyte count was not appreciably increased. Given the involvement of monocytes and macrophages in wound debridement, regulation of the inflammatory response, and stimulation of reparative processes, these findings may indicate the involvement of the mononuclear phagocyte system.

In animals treated with compound **3**, the reduction in wound area was less pronounced than that observed with compound **1** but remained greater than that in the vehicle-control group. By day 4, the wound area had decreased to 1.19 ± 0.01 cm^2, corresponding to a 31.2% reduction from baseline and a statistically significant difference compared with the vehicle-control group ($p < 0.001$). By day 8, the wound area had decreased to 0.37 ± 0.01 cm^2, representing a 78.6% reduction from baseline, and remained significantly smaller than the corresponding control value ($p < 0.001$). Thus, compound **3** exhibited a moderate wound-closure effect that was less pronounced than that of compound **1** but greater than that observed in the vehicle-control group.

In the vehicle-control group, the wound area decreased by only 8.1% during the first four days, whereas the overall reduction reached 70.5% by day 8. This pattern is consistent with the expected course of wound repair and the transition from the inflammatory to the proliferative phase.

A limitation of the present study is that wound repair was assessed primarily by macroscopic wound-area reduction, without histological evaluation of re-epithelialization, granulation tissue formation, collagen deposition and organization, or angiogenesis. Therefore, the observed differences should be interpreted as evidence of accelerated macroscopic wound closure rather than definitive demonstration of complete tissue regeneration. In addition, the study did not include an equimolar free-compound treatment arm; consequently, the current design demonstrates the effect of the compound-containing formulation as a whole but does not allow the intrinsic pharmacological effect of the compounds to be separated from formulation-dependent effects on local delivery. Histological and molecular studies, together with appropriately matched free-compound controls, will be required to establish the structural quality, mechanisms of repair, and the relative contribution of the active compounds and the carrier system.

The hematological parameters recorded at the end of the experimental period are summarized in Table 4. Compared with the vehicle-control group, WBC counts were significantly lower in animals treated with the fibrous dressings containing compound **1** or compound **3**: 4.40 ± 0.30 and 3.90 ± 0.14 versus $8.30 \pm 0.10 \times 10^9$/L, respectively ($p < 0.001$ for both comparisons). In contrast, ESR did not differ significantly among the groups and amounted to 1.10 ± 0.10, 1.20 ± 0.20, and 0.80 ± 0.20 mm/h, respectively ($p > 0.05$). Thus, ESR provided no evidence of a marked between-group difference in the systemic inflammatory response.

In animals treated with the compound **1**-containing dressing, RBC count, HGB concentration, and HCT were significantly lower than those in the vehicle-control group and amounted to $7.90 \pm 0.04 \times 10^{12}$/L, 15.20 ± 0.12 g/dL, and 42.60 ± 0.20%, respectively ($p < 0.001$). However, MCV remained close to the control value (56.20 ± 0.12 vs. 57.20 ± 0.21 fL), while MCH and MCHC were not reduced. This profile does not indicate insufficient hemoglobinization of erythrocytes. The modest increase in RDW from 13.00 ± 0.06% in the vehicle-control group to 14.10 ± 0.04% in the compound **1** group indicates slightly greater variability in erythrocyte size.

Table 4. Hematological parameters in Wistar rats at the end of the experimental period following topical treatment with PVP K-30-based fibrous dressings containing compound **1** or compound **3**.

Parameter	Compound 1	Compound 3	Vehicle Control
WBC ($\times 10^9$/L)	4.40 ± 0.30 ***	3.90 ± 0.14 ***	8.30 ± 0.10
HGB (g/dL)	15.20 ± 0.12 ***	13.30 ± 0.32 ***	21.80 ± 0.10
HCT (%)	42.60 ± 0.20 ***	48.70 ± 0.63 ***	68.10 ± 0.63
RBC ($\times 10^{12}$/L)	7.90 ± 0.04 ***	9.50 ± 0.07 ***	12.00 ± 0.16
MCV (fL)	56.20 ± 0.12 **	51.10 ± 0.04 ***	57.20 ± 0.21
MCH (pg)	18.90 ± 0.04 **	13.80 ± 0.22 ***	18.40 ± 0.14
MCHC (g/dL)	35.40 ± 0.20 ***	27.40 ± 0.29 ***	32.40 ± 0.14
RDW (%)	14.10 ± 0.04 ***	13.10 ± 0.04	13.00 ± 0.06
PLT ($\times 10^9$/L)	997.10 ± 0.71 ***	1087.40 ± 2.60 ***	724.20 ± 1.27
MPV (fL)	8.20 ± 0.14 ***	9.10 ± 0.07	9.50 ± 0.16
ESR (mm/h)	1.10 ± 0.10	1.20 ± 0.20	0.80 ± 0.20

Note: Data are presented as mean ± SEM (n = 5 biologically independent animals per group). Statistical significance was assessed relative to the vehicle-control group: ** $p < 0.01$, and *** $p < 0.001$. The vehicle-control group received a blank PVP K-30-based fibrous dressing without the investigated compounds. WBC, white blood cell count; RBC, red blood cell count; HGB, hemoglobin; HCT, hematocrit; MCV, mean corpuscular volume; MCH, mean corpuscular hemoglobin; MCHC, mean corpuscular hemoglobin concentration; RDW, red blood cell distribution width; PLT, platelet count; MPV, mean platelet volume; ESR, erythrocyte sedimentation rate.

In the compound **3** group, RBC count, HGB, and HCT were 9.50 ± 0.07 × 10^{12}/L, 13.30 ± 0.32 g/dL, and 48.70 ± 0.63%, respectively. MCV, MCH, and MCHC were also significantly lower than the corresponding vehicle-control values and amounted to 51.10 ± 0.04 fL, 13.80 ± 0.22 pg, and 27.40 ± 0.29 g/dL, respectively ($p < 0.001$). The concurrent decreases in MCH and MCHC suggest reduced erythrocyte hemoglobinization and a shift toward a hypochromic erythrocyte profile.

Platelet counts were significantly higher in the compound **1** and compound **3** groups than in the vehicle-control group: 997.10 ± 0.71 and 1087.40 ± 2.60 versus 724.20 ± 1.27 × 10^9/L, respectively ($p < 0.001$). These values correspond to increases of 37.7% and 50.2%, respectively. MPV was significantly lower only in the compound **1** group (8.20 ± 0.14 vs. 9.50 ± 0.16 fL; $p < 0.001$), whereas no significant difference was observed between the compound **3** and vehicle-control groups.

Overall, treatment with the compound **1**-containing dressing was not associated with a hypochromic erythrocyte pattern, despite significant differences in several erythrocyte-related indices, lower WBC counts, and higher platelet counts relative to the vehicle control. Compound **3** produced a more pronounced reduction in erythrocyte hemoglobinization indices, which warrants cautious interpretation. The absence of significant ESR changes does not indicate a marked systemic inflammatory response as assessed by this parameter. At the same time, the high RBC, HGB, and HCT values observed in the vehicle-control group may reflect hemoconcentration or study-specific preanalytical factors.

Taken together, the hematological findings in the compound **3** group were characterized by lower erythrocyte hemoglobinization indices and total WBC count, together with a higher platelet count, relative to the vehicle-control group. The reductions in MCV, MCH, and MCHC suggest a shift toward a hypochromic erythrocyte profile; however, these findings should be interpreted cautiously in view of the unusually high RBC, HGB, and HCT values observed in the vehicle-control group.

The differential leukocyte counts are presented in Table 5. Promyelocytes, myelocytes, metamyelocytes, myeloblasts, band neutrophils, basophils, and plasma cells were not detected in the peripheral blood of animals from any group. The absence of circulating

immature granulocytes and blast cells indicates that no marked left shift in the differential leukocyte count was present at the time of analysis.

Table 5. Differential leukocyte counts in Wistar rats at the end of the experimental period.

Leukocyte Type	Vehicle Control (n = 5)	Compound 1 (n = 5)	Compound 3 (n = 5)
Segmented neutrophils (%)	14.10 ± 0.04	22.40 ± 0.13 ***	25.20 ± 0.06 ***
Monocytes (%)	5.00 ± 0.02	10.10 ± 0.06 ***	4.00 ± 0.06 ***
Lymphocytes (%)	78.90 ± 0.32	66.50 ± 0.45 ***	69.80 ± 0.56 ***
Eosinophils (%)	2.00 ± 0.32	1.00 ± 0.32	1.00 ± 0.32

Note: Data are presented as mean ± SEM (n = 5 biologically independent animals per group). *** $p < 0.001$ versus the vehicle-control group. Basophils, band neutrophils, immature granulocytic cells (promyelocytes, myelocytes, and metamyelocytes), plasma cells, and blast cells were not detected in the peripheral blood of animals from any group.

The relative proportions of segmented neutrophils were significantly higher in the compound **1** and compound **3** groups, reaching 22.40 ± 0.13% and 25.20 ± 0.06%, respectively, compared with 14.10 ± 0.04% in the vehicle-control group ($p < 0.001$). However, total WBC counts in both treatment groups were approximately half that observed in the vehicle-control group.

In the compound **1** group, the relative proportion of monocytes was 10.10 ± 0.06%, which was higher than that in the vehicle-control group (5.00 ± 0.02%; $p < 0.001$). Nevertheless, when the lower total WBC count is taken into account, these findings do not indicate a marked increase in the absolute monocyte count. In the compound **3** group, the relative proportion of monocytes was lower than that in the vehicle-control group (4.00 ± 0.06 vs. 5.00 ± 0.02%; $p < 0.001$).

Lymphocytes remained the predominant circulating leukocyte population in all groups, which is characteristic of rats. Their relative proportions were lower in the compound **1** and compound **3** groups, accounting for 66.50 ± 0.45% and 69.80 ± 0.56%, respectively, compared with 78.90 ± 0.32% in the vehicle-control group ($p < 0.001$).

The proportion of eosinophils was low and did not differ significantly among the groups, accounting for 1.00 ± 0.32% in both treatment groups and 2.00 ± 0.32% in the vehicle-control group. Thus, no eosinophilia was observed.

Overall, the differential leukocyte profile was characterized by a higher relative proportion of segmented neutrophils and a correspondingly lower proportion of lymphocytes in the compound **1** and compound **3** groups. Because total WBC counts were lower in both treatment groups, these relative changes do not indicate absolute neutrophilia or a pronounced systemic inflammatory response. The findings indicate a moderate redistribution of circulating leukocyte populations without the appearance of immature cells in the peripheral blood.

The serum biochemical parameters measured at the end of the experimental period are summarized in Table 6. Serum albumin concentrations did not differ significantly among the groups. Total protein was unchanged in the compound **1** group, whereas a modest increase was observed in the compound **3** group compared with the vehicle control. The albumin/globulin ratio was modestly lower in the compound **1** group, whereas no significant difference was observed in the compound **3** group.

Table 6. Serum biochemical parameters in Wistar rats at the end of the experimental period.

Parameter	Vehicle Control	Compound 1	Compound 3
Albumin (g/L)	35.00 ± 0.40	34.00 ± 0.56	35.00 ± 0.63
Total protein (g/L)	70.00 ± 0.40	69.00 ± 1.27	74.00 ± 1.41 *
ALP (U/L)	657.00 ± 2.35	1216.00 ± 4.90 ***	403.00 ± 3.16 ***
ALT (U/L)	49.00 ± 0.40	73.00 ± 0.56 ***	46.00 ± 0.35 ***
AST (U/L)	211.00 ± 0.63	209.00 ± 1.43	278.00 ± 1.27 ***
LDH (U/L)	3255.00 ± 5.10	1668.00 ± 6.39 ***	4256.00 ± 4.15 ***
GGT (U/L)	2.00 ± 0.03	3.00 ± 0.32 *	1.00 ± 0.28 **
Creatinine (µmol/L)	43.00 ± 0.40	45.00 ± 0.63 *	46.00 ± 0.35 ***
Urea (mmol/L)	7.20 ± 0.68	5.90 ± 0.32	3.70 ± 0.68 **
Glucose (mmol/L)	7.00 ± 0.40	6.70 ± 0.60	8.60 ± 0.51 *
Total cholesterol (mmol/L)	2.18 ± 0.01	2.27 ± 0.06	2.75 ± 0.08 ***
Triglycerides (mmol/L)	1.98 ± 0.01	0.71 ± 0.08 ***	0.78 ± 0.09 ***
α-Amylase (U/L)	6591.00 ± 5.10	5701.00 ± 20.10 ***	6124.00 ± 8.48 ***
Total bilirubin (µmol/L)	5.00 ± 0.28	5.00 ± 0.63	6.00 ± 0.28 *
Direct bilirubin (µmol/L)	2.00 ± 0.28	2.00 ± 0.35	2.00 ± 0.35
Indirect bilirubin (µmol/L)	3.00 ± 0.56	3.00 ± 0.32	4.00 ± 0.28
Uric acid (µmol/L)	177.00 ± 0.40	178.00 ± 0.63	278.00 ± 0.63 ***
Inorganic phosphorus (mmol/L)	2.33 ± 0.26	1.97 ± 0.30	1.95 ± 0.28
Total calcium (mmol/L)	2.28 ± 0.01	2.54 ± 0.01 ***	2.55 ± 0.05 ***
Albumin fraction (%)	49.10 ± 0.06	47.70 ± 0.06 ***	48.80 ± 0.04 **
Globulin fraction (%)	50.90 ± 0.06	52.30 ± 0.06 ***	51.20 ± 0.04 **
Albumin/globulin ratio	0.96 ± 0.006	0.91 ± 0.006 ***	0.95 ± 0.006

Note: Data are presented as mean ± SEM (n = 5 biologically independent animals per group). Statistical significance was assessed relative to the vehicle-control group: * $p < 0.05$, ** $p < 0.01$, and *** $p < 0.001$. ALP, alkaline phosphatase; ALT, alanine aminotransferase; AST, aspartate aminotransferase; LDH, lactate dehydrogenase; GGT, gamma-glutamyl transferase.

Treatment with the compound **1**-containing dressing was associated with significantly higher ALP, ALT, and GGT activities than those recorded in the vehicle-control group. ALP activity increased from 657.00 ± 2.35 to 1216.00 ± 4.90 U/L ($p < 0.001$), ALT increased from 49.00 ± 0.40 to 73.00 ± 0.56 U/L ($p < 0.001$), and GGT increased from 2.00 ± 0.03 to 3.00 ± 0.32 U/L ($p < 0.05$). In contrast, AST activity remained unchanged, while LDH activity was significantly lower than that in the vehicle-control group.

The compound **3** group displayed a different enzymatic profile. AST and LDH activities were significantly higher than the corresponding vehicle-control values, reaching 278.00 ± 1.27 and 4256.00 ± 4.15 U/L, respectively ($p < 0.001$). Conversely, ALP, ALT, and GGT activities were lower than those in the vehicle-control group.

Creatinine concentrations were slightly but significantly higher in the compound **1** and compound **3** groups than in the vehicle-control group (45.00 ± 0.63 and 46.00 ± 0.35 vs. 43.00 ± 0.40 µmol/L, respectively; $p < 0.05$ and $p < 0.001$, respectively). However, these increases were small and were not accompanied by increased urea concentrations. Urea was unchanged in the compound **1** group and significantly lower in the compound **3** group. Therefore, the combined creatinine and urea profiles do not indicate a consistent pattern of impaired renal excretory function.

Glucose was unchanged in the compound **1** group, whereas a modest increase was observed in the compound **3** group compared with the vehicle control. Total cholesterol was significantly higher in the compound **3** group (2.75 ± 0.08 vs. 2.18 ± 0.01 mmol/L; $p < 0.001$), whereas no significant change was detected in the compound **1** group. Triglyceride concentrations were significantly lower in both treatment groups than in the vehicle-

control group ($p < 0.001$), indicating treatment-associated changes in the circulating lipid profile.

Serum α-amylase activity was significantly lower in the compound **1** and compound **3** groups than in the vehicle-control group. Total bilirubin was modestly higher in the compound **3** group than in the vehicle-control group, whereas direct and indirect bilirubin concentrations did not differ significantly. Overall, these findings did not indicate a consistent pattern of impaired bilirubin conjugation or excretion.

Uric acid was unchanged in the compound **1** group but was significantly higher in the compound **3** group (278.00 ± 0.63 vs. 177.00 ± 0.40 µmol/L; $p < 0.001$). This isolated increase may indicate altered purine metabolism or tissue turnover.

Inorganic phosphorus concentrations did not differ significantly among the groups. In contrast, total calcium concentrations were moderately but significantly higher in both treatment groups than in the vehicle-control group ($p < 0.001$). These findings indicate a modest treatment-associated change in calcium homeostasis without a corresponding significant alteration in serum phosphorus.

Overall, the two investigated compounds produced distinct biochemical profiles. Compound **1** was associated primarily with increased ALP, ALT, and GGT activities, whereas compound **3** was associated with increased AST, LDH, uric acid, and total cholesterol concentrations. Nevertheless, neither treatment produced a consistent biochemical pattern of impaired hepatic synthetic or excretory function or marked renal dysfunction. The unusually high RBC, HGB, and HCT values in the vehicle-control group may reflect hemoconcentration or preanalytical variability. The increased ALP, ALT, and GGT activities observed with compound **1** indicate a treatment-associated biochemical response; however, no consistent pattern of hepatic synthetic/excretory dysfunction or renal dysfunction was observed.

4. Conclusions

This study combined free-energy simulations, computational and experimental acute-toxicity assessments, and an in vivo excisional wound model to evaluate the biological potential of the investigated compounds. The PMF analysis revealed distinct interactions with the stratum corneum lipid model: compound 1 showed pronounced lipid partitioning and potential intramembrane retention, whereas compounds **2** and **3** encountered broad free-energy barriers within the membrane interior. The acute-toxicity results provided the basis for selecting compounds for subsequent wound-healing evaluation. Compound **2** consistently exhibited the highest acute toxicity in both the rat and *Danio rerio* models and was therefore excluded from further investigation. In contrast, compounds **1** and **3** demonstrated comparatively more favorable acute-toxicity profiles and were selected for topical evaluation. PVP K-30-based fibrous dressings containing either compound significantly accelerated wound-area reduction compared with the blank vehicle dressing. The greatest effect was observed for compound **1**, which reduced the wound area by 89.0% by day 8, compared with 78.6% for compound **3** and 70.5% for the vehicle control. Neither treatment caused clinically evident deterioration in the animals. Nevertheless, the lower total WBC counts, higher platelet counts, altered erythrocyte indices in the compound **3** group, and compound-specific changes in serum enzyme activities and metabolic parameters demonstrate that wound-closure efficacy should not be interpreted as evidence of complete systemic safety. At the same time, the absence of a consistent pattern across hepatic synthetic/excretory and renal-function-related markers provided no evidence of overt systemic organ dysfunction during the observation period. Overall, the compound **1**-containing fibrous dressing demonstrated the most pronounced effect

on macroscopic wound-area reduction and should be prioritized for further histological, mechanistic, and longer-term safety evaluation.

Supplementary Materials: The following supporting information can be downloaded at: https://www.mdpi.com/article/10.3390/scipharm94040093/s1, Section S1: Molecular Dynamics and Accelerated Weight Histogram Calculations [23,27]; Table S1: Molecular composition of the stratum corneum model; Table S2: Permeants and system-specific simulation parameters; Section S2: Experimental Acute-Toxicity Data; Section S3: Application of the Electrospun Fibrous Dressing [47]; Figure S1: Application of the PVP K-30-based electrospun fibrous dressing in the rat wound model; Section S4: Individual Wound-Area Data and Statistical Analysis; Table S3: Individual wound-area measurements (cm^2) for each animal on Days 0, 4, and 8; Table S4: Two-way mixed repeated-measures ANOVA of wound-area dynamics; Table S5: One-way ANOVA at individual assessment time points; Table S6: Dunnett-adjusted comparisons with the vehicle-control group. Supplementary References.

Author Contributions: Conceptualization, Y.K.; methodology, Y.K., B.K., L.K., O.I., I.P., T.C. and M.S.; software, Y.K.; validation, Y.K., V.P., B.K., L.K., O.I., T.C. and M.S.; formal analysis, Y.K., D.S. and M.S.; investigation, Y.K., B.K., O.I., I.P., T.C., D.S. and M.S.; resources, V.P., B.K., L.K., O.I., I.P. and M.S.; data curation, Y.K. and M.S.; writing—original draft preparation, Y.K.; writing—review and editing, Y.K., V.P., B.K., L.K., O.I., I.P., T.C., D.S. and M.S.; visualization, Y.K.; supervision, V.P., B.K. and L.K.; project administration, Y.K.; funding acquisition, Y.K. All authors have read and agreed to the published version of the manuscript.

Funding: This research was funded by the National Research Foundation of Ukraine under project No. 2025.05/0022, "Hybrid compounds of 1,2,4-triazole and orotic acid with radioprotective, wound-healing, and regenerative properties for the needs of civilians and the Armed Forces of Ukraine." The study was also conducted within the framework of the state-funded research project of the Ministry of Health of Ukraine, state registration No. 0126U001480, "Development of 1,2,4-triazole derivatives with polypharmacological activity for the needs of military medicine and persons affected by hostilities."

Institutional Review Board Statement: The animal study protocol was reviewed and approved by the Commission on Bioethics of Poltava State Agrarian University (Protocol No. 1 C/I, approved on 12 January 2026). All procedures involving animals were conducted in accordance with applicable national bioethical requirements, Directive 2010/63/EU, the European Convention for the Protection of Vertebrate Animals Used for Experimental and Other Scientific Purposes (ETS No. 123), and the principles of replacement, reduction, and refinement (3Rs).

Informed Consent Statement: Not applicable.

Data Availability Statement: The data presented in this study are available in the article and its Supplementary Materials. Molecular-dynamics input files, time-resolved AWH outputs, derived PMF profiles, convergence diagnostics, and analysis documentation are available in the Zenodo repository at https://doi.org/10.5281/zenodo.22255611.

Conflicts of Interest: The authors declare no conflicts of interest.

References

1. Kazmirchuk, A.; Yarmoliuk, Y.; Lurin, I.; Gybalo, R.; Burianov, O.; Derkach, S.; Karpenko, K. Ukraine's experience with management of combat casualties using NATO's four-tier "Changing as Needed" healthcare system. *World J. Surg.* **2022**, *46*, 2858–2862. [CrossRef]
2. Holubnycha, V.M.; Kholodylo, O.V. War impact on antimicrobial resistance and bacteriological profile of wound infections in Ukraine. *Commun. Med.* **2025**, *5*, 394. [CrossRef]
3. Rodrigues, M.; Kosaric, N.; Bonham, C.A.; Gurtner, G.C. Wound healing: A cellular perspective. *Physiol. Rev.* **2019**, *99*, 665–706. [CrossRef]
4. Landén, N.X.; Li, D.; Ståhle, M. Transition from inflammation to proliferation: A critical step during wound healing. *Cell. Mol. Life Sci.* **2016**, *73*, 3861–3885. [CrossRef]

5. Las Heras, K.; Garcia-Orue, I.; Rancan, F.; Igartua, M.; Santos-Vizcaino, E.; Hernandez, R.M. Modulating the immune system towards a functional chronic wound healing: A biomaterials and nanomedicine perspective. *Adv. Drug Deliv. Rev.* **2024**, *210*, 115342. [CrossRef]
6. Peddibhotla, S.; Caples, K.; Mehta, A.; Chen, Q.-Y.; Hu, J.; Idlett-Ali, S.; Zhang, L.; Zgheib, C.; Xu, J.; Liechty, K.W.; et al. Triazolothiadiazine derivative positively modulates CXCR4 signaling and improves diabetic wound healing. *Biochem. Pharmacol.* **2023**, *216*, 115764. [CrossRef]
7. Kucherenko, L.I.; Karpenko, Y.V.; Ohloblina, M.V.; Zazharskyi, V.V.; Bilan, M.V.; Kulishenko, O.M.; Bushuieva, I.V.; Parchenko, V.V. Monitoring the properties of 1,2,4-triazole derivatives for the development of original antimicrobial drugs. *Zaporozhye Med. J.* **2024**, *26*, 481–489. [CrossRef]
8. Kachaeva, M.V.; Obernikhina, N.V.; Veligina, E.S.; Zhuravlova, M.Y.; Prostota, Y.O.; Kachkovsky, O.D.; Brovarets, V.S. Estimation of biological affinity of nitrogen-containing conjugated heterocyclic pharmacophores. *Chem. Heterocycl. Compd.* **2019**, *55*, 448–454. [CrossRef]
9. Löffler, M.; Carrey, E.A.; Zameitat, E. Orotic acid, more than just an intermediate of pyrimidine de novo synthesis. *J. Genet. Genom.* **2015**, *42*, 207–219. [CrossRef]
10. Bjørklund, G.; Drapak, I.; Zimenkovsky, B.; Shanaida, M.; Kobylinska, L.; Denefil, O.; Lysiuk, R.; Pokryshko, O.; Logoyda, L.; Oliinyk, P.; et al. The role of vitamins, magnesium, and trace elements in COVID-19 treatment and post-COVID-19 rehabilitation: An updated overview. *Curr. Med. Chem.* **2025**, *32*, 3134–3154. [CrossRef]
11. Karpenko, Y.; Parchenko, V.; Kucherenko, L.; Chetvertak, T.; Bihdan, O.; Pukhalska, I.; Roik, O.; Safronova, D.; Meladze, I.; Bushueva, I. Orotic acid–1,2,4-triazole hybrids as potential MMP-2,9 modulating wound-healing agents: Synthesis, molecular docking and biological evaluation. *Sci. Pharm.* **2026**, *94*, 65. [CrossRef]
12. Karpenko, Y.; Medvedeva, K.; Solomennyi, A.; Rudenko, O.; Panasenko, O.; Parchenko, V.; Vasyuk, S. Design, synthesis, molecular docking, and antioxidant properties of a series of new S-derivatives of ((1,2,4-triazol-3(2H)-yl)methyl)thiopyrimidines. *Sci. Pharm. Sci.* **2025**, *1*, 62–70. [CrossRef]
13. Karpenko, Y.; Parchenko, V.; Panasenko, O.; Bihdan, O.; Pukhalska, I.; Nikiforov, O.; Nahorna, N.; Nahornyi, V.; Roik, O. Novel 1,2,4-triazole–thiopyrimidine hybrids as COX-2 inhibitors: Synthesis, ADME profiling, antioxidant activity, and molecular docking. *BioMed Res. Int.* **2026**, *2026*, 4477854. [CrossRef]
14. Abrigo, M.; McArthur, S.L.; Kingshott, P. Electrospun nanofibers as dressings for chronic wound care: Advances, challenges, and future prospects. *Macromol. Biosci.* **2014**, *14*, 772–792. [CrossRef]
15. Kou, J.; Li, Y.; Zhou, C.; Wang, X.; Ni, J.; Lin, Y.; Ge, H.; Zheng, D.; Chen, G.; Sun, X.; et al. Electrospinning in promoting chronic wound healing: Materials, process, and applications. *Front. Bioeng. Biotechnol.* **2025**, *13*, 1550553. [CrossRef]
16. Ignatova, M.; Rashkov, I.; Manolova, N. Drug-loaded electrospun materials in wound-dressing applications and in local cancer treatment. *Expert Opin. Drug Deliv.* **2013**, *10*, 469–483. [CrossRef]
17. Rasekh, M.; Karavasili, C.; Soong, Y.L.; Bouropoulos, N.; Morris, M.; Armitage, D.; Li, X.; Fatouros, D.G.; Ahmad, Z. Electrospun PVP–indomethacin constituents for transdermal dressings and drug-delivery devices. *Int. J. Pharm.* **2014**, *473*, 95–104. [CrossRef]
18. Rahmani, F.; Ziyadi, H.; Baghali, M.; Luo, H.; Ramakrishna, S. Electrospun PVP/PVA nanofiber mat as a novel potential transdermal drug-delivery system for buprenorphine: A solution needed for pain management. *Appl. Sci.* **2021**, *11*, 2779. [CrossRef]
19. Cheng, S.; Wang, H.; Pan, X.; Zhang, C.; Zhang, K.; Chen, Z.; Dong, W.; Xie, A.; Qi, X. Dendritic Hydrogels with Robust Inherent Antibacterial Properties for Promoting Bacteria-Infected Wound Healing. *ACS Appl. Mater. Interfaces* **2022**, *14*, 11144–11155. [CrossRef]
20. Zeng, Q.; Qi, X.; Shi, G.; Zhang, M.; Haick, H. Wound Dressing: From Nanomaterials to Diagnostic Dressings and Healing Evaluations. *ACS Nano* **2022**, *16*, 1708–1733. [CrossRef]
21. Lundborg, M.; Narangifard, A.; Wennberg, C.L.; Lindahl, E.; Norlén, L. Human skin barrier structure and function analyzed by cryo-electron microscopy and molecular dynamics simulation. *J. Struct. Biol.* **2018**, *203*, 149–161. [CrossRef]
22. Lundborg, M.; Wennberg, C.L.; Narangifard, A.; Lindahl, E.; Norlén, L. Predicting drug permeability through skin using molecular dynamics simulation. *J. Control. Release* **2018**, *283*, 269–279. [CrossRef]
23. Lundborg, M.; Lidmar, J.; Hess, B. The accelerated weight histogram method for alchemical free-energy calculations. *J. Chem. Phys.* **2021**, *154*, 204103. [CrossRef]
24. Karpenko, Y.V.; Panasenko, O.I.; Zazharsky, V.V.; Parchenko, V.V.; Pidlisny, O.V.; Yaroshenko, I.V.; Bilan, M.V.; Davydenko, P.O.; Kulishenko, O.M.; Zazharska, N.M. Synthesis, chemical properties and search for molecular descriptors of the fungicidal activity of new hybrids of 1,2,4-triazole (1,3,4-oxadiazole) bearing a pyrimidine fragment. *Vopr. Khim. Khim. Tekhnol.* **2025**, *4*, 58–69. [CrossRef]

25. Das, C.; Noro, M.G.; Olmsted, P.D. Simulation studies of stratum corneum lipid mixtures. *Biophys. J.* **2009**, *97*, 1941–1951. [CrossRef]
26. Notman, R.; Anwar, J.; Briels, W.J.; Noro, M.G.; den Otter, W.K. Simulations of skin barrier function: Free energies of hydrophobic and hydrophilic transmembrane pores in ceramide bilayers. *Biophys. J.* **2008**, *95*, 4763–4771. [CrossRef]
27. Lundborg, M.; Wennberg, C.; Lindahl, E.; Norlén, L. Simulating the skin permeation process of ionizable molecules. *J. Chem. Inf. Model.* **2024**, *64*, 5295–5302. [CrossRef]
28. Klauda, J.B.; Venable, R.M.; Freites, J.A.; O'Connor, J.W.; Tobias, D.J.; Mondragon-Ramirez, C.; Vorobyov, I.; MacKerell, A.D., Jr.; Pastor, R.W. Update of the CHARMM all-atom additive force field for lipids: Validation on six lipid types. *J. Phys. Chem. B* **2010**, *114*, 7830–7843. [CrossRef]
29. Vanommeslaeghe, K.; Hatcher, E.; Acharya, C.; Kundu, S.; Zhong, S.; Shim, J.; Darian, E.; Guvench, O.; Lopes, P.; Vorobyov, I.; et al. CHARMM General Force Field: A Force Field for Drug-Like Molecules Compatible with the CHARMM All-Atom Additive Biological Force Fields. *J. Comput. Chem.* **2010**, *31*, 671–690. [CrossRef]
30. Karpenko, Y.; Omelyanchik, L.; Panasenko, T. Experimental and theoretical spectroscopic study of thione–thiol tautomerism of new hybrides 1,3,4-oxadiazole-2-thion with acridine-9(10H)-one. *Chem. Chem. Technol.* **2018**, *12*, 419–428. [CrossRef]
31. Lindahl, V.; Lidmar, J.; Hess, B. Accelerated weight histogram method for exploring free energy landscapes. *J. Chem. Phys.* **2014**, *141*, 044110. [CrossRef]
32. Venable, R.M.; Krämer, A.; Pastor, R.W. Molecular dynamics simulations of membrane permeability. *Chem. Rev.* **2019**, *119*, 5954–5997. [CrossRef]
33. Pires, D.E.V.; Blundell, T.L.; Ascher, D.B. pkCSM: Predicting small-molecule pharmacokinetic and toxicity properties using graph-based signatures. *J. Med. Chem.* **2015**, *58*, 4066–4072. [CrossRef]
34. U.S. Environmental Protection Agency. Toxicity Estimation Software Tool (TEST), Version 5.1.2. Available online: https://www.epa.gov/comptox-tools/toxicity-estimation-software-tool-test (accessed on 1 September 2026).
35. Myrko, I.; Chaban, T.; Demchuk, Y.; Drapak, Y.; Chaban, I.; Drapak, I.; Pankiv, M.; Matiychuk, V. Current trends of chemoinformatics and computer chemistry in drug design: A review. *Curr. Chem. Lett.* **2024**, *13*, 151–162. [CrossRef]
36. Trush, M.M.; Kovalishyn, V.; Ocheretniuk, A.D.; Kobzar, O.L.; Kachaeva, M.V.; Brovarets, V.S.; Metelytsia, L.O. QSAR study of some 1,3-oxazolylphosphonium derivatives as new potent anti-Candida agents and their toxicity evaluation. *Curr. Drug Discov. Technol.* **2019**, *16*, 204–209. [CrossRef]
37. Achar, J.; Firman, J.W.; Cronin, M.T.D. Conservative consensus QSAR approach for the prediction of rat acute oral toxicity. *Comput. Toxicol.* **2025**, *35*, 100374. [CrossRef]
38. Organisation for Economic Co-operation and Development (OECD). *Test No. 203: Fish, Acute Toxicity Test*; OECD Guidelines for the Testing of Chemicals, Section 2; OECD Publishing: Paris, France, 2019. [CrossRef]
39. AAT Bioquest; Inc. Quest Graph™ LC50 Calculator. Available online: https://www.aatbio.com/tools/lc50-calculator (accessed on 1 September 2026).
40. Organisation for Economic Co-operation and Development (OECD). *Test No. 425: Acute Oral Toxicity: Up-and-Down Procedure*; OECD Guidelines for the Testing of Chemicals, Section 4; OECD Publishing: Paris, France, 2022. [CrossRef]
41. U.S. Environmental Protection Agency. Acute Oral Toxicity Up-and-Down Procedure: AOT425StatPgm. Available online: https://www.epa.gov/pesticide-science-and-assessing-pesticide-risks/acute-oral-toxicity-and-down-procedure (accessed on 1 September 2026).
42. United Nations. *Globally Harmonized System of Classification and Labelling of Chemicals (GHS)*, 11th ed.; United Nations: New York, NY, USA; Geneva, Switzerland, 2025; ST/SG/AC.10/30/Rev.11. Available online: https://unece.org/transport/dangerous-goods/ghs-rev11-2025 (accessed on 1 September 2026).
43. European Parliament; Council of the European Union. Directive 2010/63/EU of 22 September 2010 on the Protection of Animals Used for Scientific Purposes. *Off. J. Eur. Union* **2010**, *L276*, 33–79. Available online: https://eur-lex.europa.eu/eli/dir/2010/63/oj (accessed on 1 September 2026).
44. Council of Europe. *European Convention for the Protection of Vertebrate Animals Used for Experimental and Other Scientific Purposes*; ETS No. 123; Council of Europe: Strasbourg, France, 1986. Available online: https://www.coe.int/en/web/conventions/full-list?module=treaty-detail&treatynum=123 (accessed on 1 September 2026).
45. Ishchenko, O.V.; Vlasenko, I.O.; Shmatenko, O.P.; Solomennyi, A.M.; Roik, O.M. The pharmacotechnological study for the development of applicatic anesthetic medicinal films. *Ukr. J. Mil. Med.* **2025**, *6*, 177–187. [CrossRef]
46. Almasi, L.; Arkan, E.; Farzaei, M.H.; Iranpanah, A.; Jalili, C.; Abbaszadeh, F.; Aghaz, F.; Fakhri, S.; Echeverría, J. Preparation of *Tragopogon graminifolius*-loaded electrospun nanofibers and evaluating its wound healing activity in a rat model of skin scar. *Front. Pharmacol.* **2025**, *16*, 1533010. [CrossRef]
47. Kundin, J.I. A new way to size up a wound. *Am. J. Nurs.* **1989**, *89*, 206–207. [CrossRef]

48. AnalystSoft Inc. BioStat. Available online: https://www.analystsoft.com/en/products/biostat/ (accessed on 2 September 2026).
49. MedCalc Software Ltd. MedCalc Statistical Software. Available online: https://www.medcalc.org (accessed on 2 September 2026).

Disclaimer/Publisher's Note: The statements, opinions and data contained in all publications are solely those of the individual author(s) and contributor(s) and not of MDPI and/or the editor(s). MDPI and/or the editor(s) disclaim responsibility for any injury to people or property resulting from any ideas, methods, instructions or products referred to in the content.